AIP | Journal of Applied Physics

Optical and vibrational properties of (ZnO)k In2O3 natural superlattice nanostructures

Samuel Margueron, Jan Pokorny, Stella Skiadopoulou, Stanislav Kamba, Xin Liang, and David R. Clarke

Citation: Journal of Applied Physics **119**, 195103 (2016); doi: 10.1063/1.4950789
View online: http://dx.doi.org/10.1063/1.4950789
View Table of Contents: http://scitation.aip.org/content/aip/journal/jap/119/19?ver=pdfcov
Published by the AIP Publishing

Optical and vibrational properties of $(ZnO)_k In_2O_3$ natural superlattice nanostructures

Samuel Margueron,[1,2] Jan Pokorny,[3] Stella Skiadopoulou,[3] Stanislav Kamba,[3] Xin Liang,[4] and David R. Clarke[2]
[1]*Laboratoire Matériaux Optiques, Photonique et Systèmes, Université de Lorraine et CentraleSupélec, 57070 Metz, France*
[2]*John A. Paulson School of Engineering and Applied Sciences, Harvard University, Cambridge, Maryland 02138, USA*
[3]*Institute of Physics, Czech Academy of Sciences, Na Slovance 2, 182 21 Prague 8, Czech Republic*
[4]*School of Materials Science and Engineering, Changzhou University, Changzhou, Jiangsu Province 213164, China*

(Received 28 January 2016; accepted 23 April 2016; published online 18 May 2016)

A thermodynamically stable series of superlattices, $(ZnO)_kIn_2O_3$, form in the ZnO-In_2O_3 binary oxide system for $InO_{1.5}$ concentrations from about 13 up to about 33 mole percent (m/o). These natural superlattices, which consist of a periodic stacking of single, two-dimensional sheets of InO_6 octahedra, are found to give rise to systematic changes in the optical and vibrational properties of the superlattices. Low-frequency Raman scattering provides the evidence for the activation of acoustic phonons due to the folding of Brillouin zone. New vibrational modes at 520 and 620 cm^{-1}, not present in either ZnO or In_2O_3, become Raman active. These new modes are attributed to collective plasmon oscillations localized at the two-dimensional $InO_{1.5}$ sheets. Infrared reflectivity experiments, and simulations taking into account a negative dielectric susceptibility due to electron carriers in ZnO and interface modes of the dielectric layer of InO_2, explain the occurrence of these new modes. We postulate that a localized electron gas forms at the ZnO/InO_2 interface due to the electron band alignment and polarization effects. All our observations suggest that there are quantum contributions to the thermal and electrical conductivity in these natural superlattices. *Published by AIP Publishing.* [http://dx.doi.org/10.1063/1.4950789]

I. INTRODUCTION

A number of oxide compounds form thermodynamically stable superlattices with spacings that are detemined by their composition and typically lie in the range of 1 to ~10 nm. These compounds, variously referred to as natural superlattices, modular compounds, homologous series, or polysomatic series, self-assemble at high-temperatures. They include a wide variety of layered perovskites as well as semiconducting oxides based on ZnO, such as those between sesquoxide phases of M_2O_3 (with M = Fe, Al, Ga, and In) and the wurtzite phase of ZnO.[1–5] One of the attractions of these natural superlattices is that they exhibit low thermal conductivity because of the large linear density of interfaces that can scatter phonons. In fact, a number of them, such as the Na_2Co_4 and $(ZnO)_kIn_2O_3$ series, exhibit promising thermoelectric properties at high temperature.[6–11] Furthermore, being thermodynamically stable phases, their superlatttice spacing will not coarsen at high temperatures, and so their intrinsic nanostructuring will not degrade as other forms of nanostructuring do.

The $(ZnO)_kIn_2O_3$ series has probably been studied in more detail than any of the other natural superlattices. Structurally, it consists of periodically arranged, single sheets of InO_2 separated by k layers of ZnO, as illustrated in the crystallographic projection and high-resolution electron microscope image in Fig. 1. The stacking is perpendicular to the ZnO basal planes {0002} with all the Zn in tetrahedral sites as in the wurtzite form of ZnO. The superlattice spacing, d_{SL}, along the ZnO c-axis direction is related to the k-value by the following: $d_{SL} \approx (k+1)\, d_{\{0002\}}$, where $d_{\{0002\}}$ is the basal plane spacing of ZnO (0.260 nm for pure ZnO). The InO_2 sheets are single, two-dimensional layers formed from edge-coordinated InO_6 octahedra. So, the parallel alignment of the InO_2 sheets creates an anisotropic crystal structure. There have been a variety of reports on the electrical properties of several of the superlattices but, with the exception of small flakes of the $k=5$ compound, all the measurements have been performed on polycrystalline materials, so the effect of the two-dimensional sheets of InO_2 on the electrical properties has not been determined. The only single-crystal measurement of the $k=5$ compound indicates an almost two orders of magnitude larger electrical conductivity parallel to the {0002} ZnO basal planes than the conductivity perpendicular to them and in the InO_2 sheets. The thermal conductivity measurements reported all show decreases with indium oxide concentration but no direct relationship was established with the superlattice spacing. More recently, it has been shown that the thermal conductivity decreases with indium oxide concentration until a concentration is reached at which the superlattices form. Above this concentration, the thermal conductivity continues to decrease but much less so.[12] By fitting the temperature and indium compositional dependences of the thermal conductivity, the thermal (Kapitza) resistance of individual InO_2 sheets was found to be $\sim 5.0 \times 10^{-10}\ m^2\,K/W$.[13] This value is larger than that of interfaces in epitaxial Si–Ge superlattice, but it

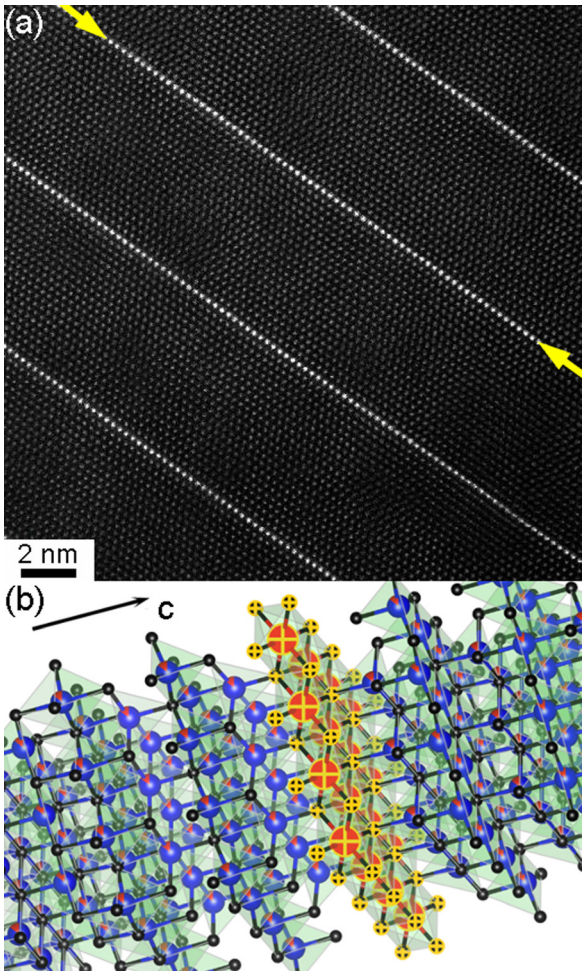

FIG. 1. (a) Aberration corrected STEM ADF image of $In_2O_3(ZnO)_k$ natural superlattice structure. The material is 10 m/o $InO_{1.5}$ annealed at 1250 °C for 7 days. The spacing between the sheets of Indium atoms, marked by the yellow arrows and shown edge on, corresponds to $k = 19$. (b) Atomic representation of a $ZnO/InO_2/ZnO$ interface. Indium ions (red) are located in the octahedral sites, with bonding oxygen ions, highlighted in yellow, to form the InO_2 sheets. The oxygen ions bond to zinc ions in tetrahedral sites on either side of the sheets creating a polarization inversion at the InO_2 sheets.

is substantially smaller than that deduced for high-angle grain boundaries in oxides. This demonstrates that the InO_2 sheets scatter phonons, presumably because of the mass density contrast with the ZnO, and, in turn, implies the possibility of confinement of those acoustic phonons having momenta along the ZnO *c*-axis. These results motivated the current work, because the Kapitza resistance does not take into account phonon dispersion and possible resonances and interferences associated with the periodicity of the superlattices and their phononic band structure.

In this work, we describe the optical and vibrational properties of a series of polycrystalline ZnO samples alloyed with *x* mole percent of $InO_{1.5}$ ranging from 0 to 33 mole percent (m/o) $InO_{1.5}$. This compositional range covers two distinct microstructural regimes.[8] At low concentrations, up to about 13 m/o $InO_{1.5}$ at 1250 °C, the indium forms point defects and clusters but no organized superlattices. (The value of the concentration at which this transition occurs is not known with any certainty but is estimated based on the microstructural observations). At higher concentrations, from about 13 m/o to 33 m/o, superlattices form at 1250 °C. This second range includes the compositions over which the $(ZnO)_kIn_2O_3$ superlattices form at 1200 °C,[4,12] namely, from $k = 11$ to $k = 3$. As the superlattices are line compounds, mixtures of two superlattices invariably form at intermediate compositions. Some of the samples were the same as those previously used in the thermal conductivity studies.[13]

To probe the superlattice structures, several complementary spectroscopies were used to characterize the polycrystalline ceramic samples. Infrared (IR) reflectivity was conducted to study the vibrational modes and the free carrier plasmon band associated with the defects and electrical conduction. Optical methods of photoluminescence and Raman spectroscopies were used to probe photoexcited electronic levels, energy transfer, and the extent of electron–phonon coupling. In addition, low frequency Raman scattering measurements were used to investigate the phonon band shape associated with the phonon confinement effects.

The organization of the paper is as follows. After a brief description of the sample preparation and optical characterization techniques, observations of the band gap absorption and resonant Raman spectroscopy using ultraviolet laser excitation (above the band gap) are described. These were used to selectively study the optical spectra of the ZnO layers. Then, the measurements by Raman spectroscopy excited with a 514.5 nm laser, i.e., in the transparent region, are presented as they show the formation of two broad and intense modes at 520 and 620 cm^{-1},[14] which we attribute to the presence of the two-dimensional indium oxide sheets, as well as confirming the confinement of the non-polar E_2 (high-frequency) modes. Following this, the low frequency Raman spectra and the new modes appearing due to the superlattice and Brillouin zone folding are then described. Finally, the possible formation of a two-dimensional electron gas at the ZnO/InO_2 interface is discussed based on the observations of electrical and optical properties of $(ZnO)_kIn_2O_3$.

II. EXPERIMENTAL DETAILS

The materials studied in this work were all polycrystalline, prepared by reacting mixed nitrate solutions and then precipitating to form ZnO powders that were pressed and sintered to full density as described in Liang and Clarke.[8] They were then annealed at 1250 °C for 7 days, so that the superlattice structure would evolve and stabilize. A series of compositions, corresponding to ZnO oxide with concentrations, *x*, of $InO_{1.5}$ (denoted as mole percent, m/o $InO_{1.5}$) from $x = 0$ to 33 were made. In addition, for comparison purposes, two pure ZnO samples were studied. One, also prepared from its nitrates was treated at 1150 °C for 1 h. The other was an undoped single crystal of ZnO grown by hydrothermal growth and provided by MTIXTL company. The crystallographic phases present in the samples were identified from the superlattice reflections in powder X-ray diffraction patterns. As summarized in Table I, samples containing between 13 m/o and 33 m/o $InO_{1.5}$ were primarily a mixture of two different superlattices, except for the 29 m/o $InO_{1.5}$ sample that was primarily the $k = 4$ superlattice.[12] X-ray diffraction also indicated that there was no preferred crystallographic

TABLE I. Composition of the $(ZnO)_kIn_2O_3$ compounds studied, the super-lattice k value from the XRD data, and measured conductivities from Hall and IR spectroscopy measurements. N.M.: not measured

Composition m/o $InO_{1.5}$	XRD Super-lattice	Values from Hall measurements: Conductivity ($S \cdot cm^{-1}$)	Values from IR measurements: Conductivity ($S \cdot cm^{-1}$)
0	None	N.M.	No plasmon
2	None	105	60
5	None	N.M.	No plasmon
8	None	68	27
10	None	N.M.	No plasmon
13	$k=9, k=11$	60	11
18	$k=7 \gg k=6$	17	13
22	$k=6, k=7$	11	11
25	$k=5 \gg k=4$	18	13
29	$k=4$	47	24
33	$k=4 \gg k=3$	141	46

texture. Examination by SEM showed that the grains were equiaxed with a grain size of approximately 10 micron. Room temperature Hall measurements were carried out in the van der Pauw geometry with hot pressed indium contacts and the results are presented in Table I. (Since these measurements are sensitive to the surface preparation, especially for polycrystalline materials, and heat treament, all the samples were prepared and annealed in the same way. Nevertheless, for this work, the precise measurements are not as significant as their systematic trends.)

For optical measurements, discs of two millimeters thick and 1.2 cm diameter were prepared and carefully optically polished to an optical finish. Diffuse optical reflectance spectra were recorded using an integrated sphere spectrophotometer (UV360, Shimadzu, Japan). The diffuse reflectance $R(E)$, with E in eV, was normalized by the spectral reflectance from a $BaSO_4$ coated etalon, and then, converted to spectral absorptivity using the Kubelka-Munk function: $F(R) = (1-R)^2/(2R) = \alpha/s$, where α is the absorptivity and s the scattering factor.

IR reflectivity spectra were recorded using an FTIR spectrometer Bruker IFS 113v over the range 30–3000 cm^{-1} with a resolution of 2 cm^{-1}. The unpolarized, near-normal reflectivity spectra $R(E)$ were recorded from optically polished surfaces of 2 mm thick ceramic disks, so that the measured spectra could be analyzed with the simple Fresnel relation. The complex dielectric permittivity was modelled as a sum of Drude terms, describing the free carrier absorption, and the Lorentzian oscillators expressing polar phonons, as described in the supplementary material. Simulations of dielectric responses and optical reflectivities were performed using Matlab® software.

Raman spectra were excited with the 514.5 nm of an Ar laser and recorded in back scattering geometry using a RENISHAW micro-Raman spectrometer equipped with Bragg filters. Laser power of ~10 mW was focused on a ~2 μm spot. The spectral resolution was better than 2 cm^{-1}. Ultraviolet and visible photoluminescence (PL) and Raman scattering were recorded on an Aramis (Horiba-Jobin-Yvon, France) micro-spectrometer with a 325 nm He-Cd laser and 532 nm solid state laser.

III. RESULTS

The absorption spectra, determined from the optical reflectivity, are shown in Fig. 2(a), for samples with compositions up to 33 m/o $InO_{1.5}$. A direct gap at 3.3 eV for pure ZnO is obtained by considering the absorption, $\alpha^2(E) \propto (E - E_g)$, to be consistent with the other reports, but the edge exhibits an Urbach tail.[15] (The Urbach tail from the pure ZnO sintered sample was so intense that a spectrum of an undoped single crystal of ZnO grown by hydrothermal method was used for the gap determination instead of ZnO ceramics spectrum seen in Fig. 2(a).) For the indium-containing samples, the absorption edges start at lower energy (3 eV) (Ref. 16) and the shift decreases to 2.6 eV with increasing indium oxide concentration, consistent with the trend previously reported.[3,5,17,18] Some discrepancies with the previous absorption measurements can probably be attributed to different optical methods and sample preparation used in Ref. 3. The latter effect emphasizes the role of carriers associated with point and substitutional defects. In addition, Fig. 2(a) shows a continuous increase in absorption below about 2 eV. As the grain size of all the samples studied is quite similar, differences in optical scattering are probably not responsible for the small discrepancy with the literature.

The UV stimulated photoluminescence for the same ten samples is shown in Fig. 2(b). The spectra indicate that the

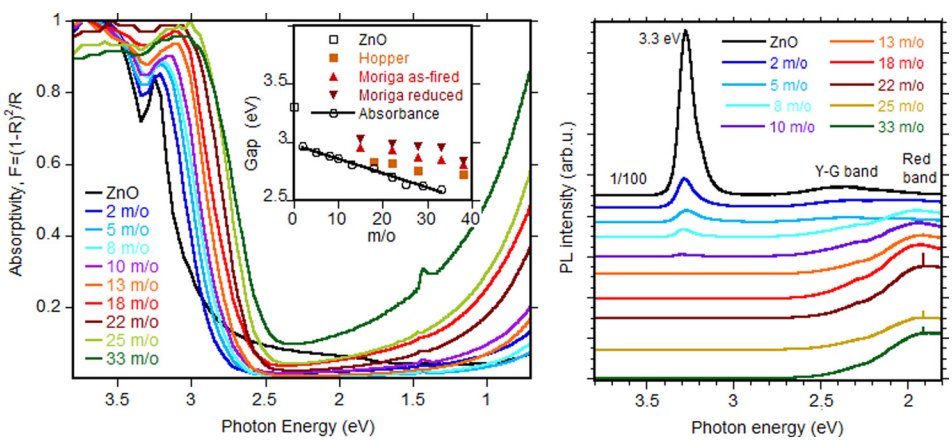

FIG. 2. (Left) Absorptivity (determined from reflectance measurements) showing the band-gap shift with the increasing indium concentration. (Right) Photoluminescence induced by a 325 nm (3.8 eV) source. The quenching of the 3.3 eV weak emission for 10 m/o of $InO_{1.5}$ is accompanied by a weak emission peak at 3.1 eV. At lower energies, the new band appears at 2 eV probably due to In–O defects. The sharp line at 1.9 eV corresponds to the second order line of the laser.

room temperature free-excitonic emission peak of pure ZnO seen at 3.3 eV quenches rapidly with indium concentration but the emission peak energy does not shift with composition.[19] Furthermore, there is no correlation with the shift of the absorption edge seen in Fig. 2(a). In addition, the deep center luminescence of ZnO occuring at 2.4 eV systematically decreases, exhibiting a new band at 2 eV with the addition of $InO_{1.5}$ above 2 m/o. The quenching of the ZnO photoluminescence with indium concentration is attibuted to the dissociation of the excitons in the presence of electronic carriers and indium point defects, clusters, or sheets.

The Raman spectra excited by an ultraviolet laser (325 nm), recorded for long acquisition times, are shown in Fig. 3. Because of the strong quenching of the photoluminescence, resonant Raman spectra are only observed from samples containing 5 m/o and more $InO_{1.5}$. Very clear, multi-order replicas of the A(LO) modes of ZnO, due to Fröhlich interactions,[20] are evident above 5 m/o. The complex first order mode will be discussed later in Fig. 4. Fitting of the 2nd up to 5th order replicas with a Pseudo-Voight function (not shown) indicates that they decrease in intensity, shift to higher energy, and also broaden with increasing the indium oxide concentration. The broadening of modes is attributed to decoherence of multi-order LO relaxation in the nanostructure, whereas the origin of the shift to high energy of the LO phonons is unclear.

The first and second order Raman spectra in the range of 100–1600 cm^{-1}, recorded at 532 nm (visible) and 325 nm (ultraviolet), for each of the compositions are compared in Fig. 4. With excitation in the visible range, all the Brillouin zone center modes of ZnO are expressed: E_2 symmetry modes (E_2(low) at 100 cm^{-1} and E_2(high) at 440 cm^{-1}) and polar modes (E_1(TO) at 420 cm^{-1}, A_1 (TO) at 385 cm^{-1}, and E_1(LO)/A_1(LO) modes at 580 cm^{-1}).[21–23] However, with increasing concentration of indium oxide, the visible

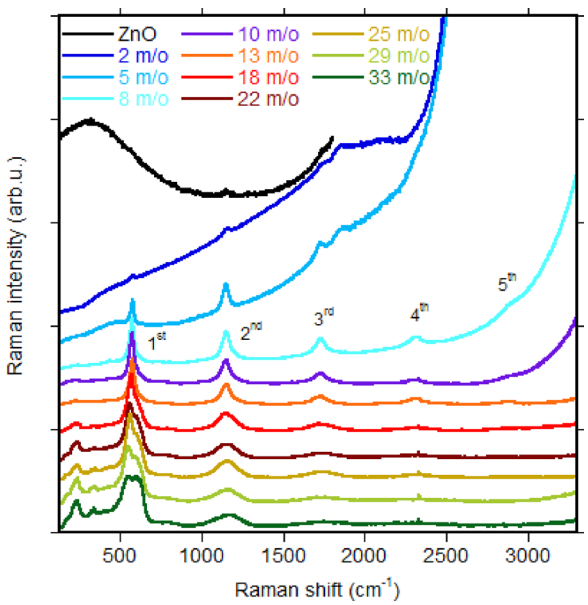

FIG. 3. Ultraviolet resonant Raman spectra of ZnO + x m/o $InO_{1.5}$ recorded at room temperature. The weak and narrow mode observed at 2300 cm^{-1} corresponds to an N_2 atmospheric Raman line. The spectra are shifted vertically relative to one another for the ease of presentation.

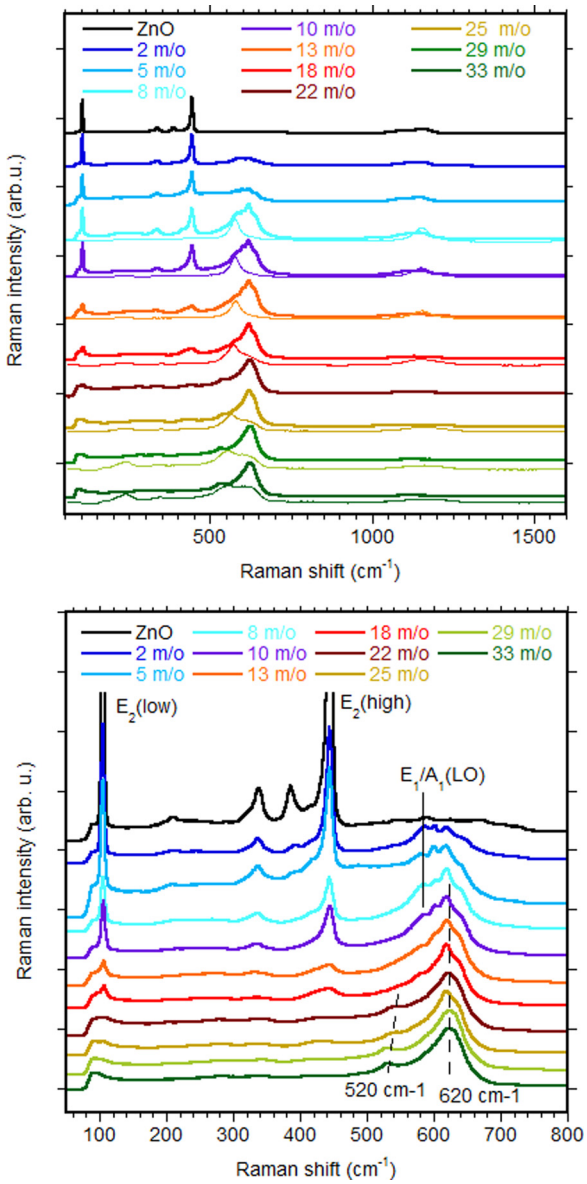

FIG. 4. (Top) Visible non-resonant Raman scattering (excited at 514.5 nm) shown in bold lines overlain with the ultraviolet resonant Raman scattering (excited at 325 nm) shown as a thin line of the first and second Raman spectra for the series of indium concentrations indicated. (Bottom) Enlargement of the visible non-resonant Raman mode in the vicinity of the 620 cm^{-1} mode.

Raman spectra flatten, giving a broad and almost constant background phonon density of states from about 100 to about 700 cm^{-1}, indicative of a "glassy" or quasi-continuum density of states. In addition, two new substantially broader modes appear at 520 and 620 cm^{-1} with increasing $InO_{1.5}$ concentration.[14] These modes are shown in greater detail in the enlargement of Fig. 4(b) recorded under visible excitation, non-resonant conditions. Fig. 4(a) also shows the ultraviolet Raman spectra for samples having concentration above 8 m/o $InO_{1.5}$. The dominant modes observed, under UV illumination, at 580 cm^{-1} and 1160 cm^{-1} (arrowed) correspond to the first and second order resonant LO mode replicas of ZnO shown in Fig. 3. Comparison of the two excitations can then be explained by the selective resonance of ZnO layers in the ultraviolet and non-resonance Raman scattering in the visible excitation. At

concentrations of 29 and 33 m/o, the two modes at 520 and 620 cm^{-1} seem to also resonate in the ultraviolet but not to produce any phonon replicas.

Enlargement of the spectra around the A_1, E_1, and E_2(high) ZnO modes obtained under non-resonant conditions at 532 nm is reproduced in Fig. 5. The intensities of the ZnO Raman modes decrease rapidly with increasing indium oxide concentration. A linear baseline has been subtracted and the intensity of the spectra has been scaled in order to compare the spectral features at different indium oxide concentrations. The non-polar E_2 (high) modes exhibit strong asymmetry and broadening with increasing indium concentration. Two regimes of phonon confinement can be identified. In the first, below 13 m/o $InO_{1.5}$, the initial E_2 (high) mode of ZnO shows a symmetric broadening and almost no shift. Based on the spatial correlation model of Parayanthal and Pollack[24] and assuming a volume confinement with a correlation radius depending on the distance to the nearest indium oxide cluster or layer sheet, it can be concluded that the confinement occurs in all the three dimensions of the Brillouin zone. As the phonon spectrum indicates that the phonon dispersion increases along the x-axis and decreases along the c-axis,[22] the broadening occurs on both the sides of E_2 (high) mode. The A_1 mode vanishes almost completely due to the confinement along the z-axis since the phonon spectrum exhibits a high dispersion and only a small density of states. In the second regime, above 13 m/o of $InO_{1.5}$, the E_2 (high) mode downshifts and broadens. It merges in between E_1 and E_2 (high) as can be seen in the spectra from the 29 m/o or 33 m/o samples. The presence of regular indium oxide layer creates a strong confinement in the z (c-axis) direction. The shift follows the confinement of the dispersion branch in the k_z (A) direction in the Brillouin zone. The new mode corresponds to an out-of-Brillouin zone center mode with a high density of states (flat band curvature). In both regimes, a confinement mechanism can be invoked in which phonons out of the Brillouin zone center participate in the Raman scattering. Together these are consistent with the increase of the background level, observed in Fig. 4, corresponding to the phonon density of states.

Complementary IR reflectivity measurements were made after carefully polishing the samples. The results are shown in Fig. 6. As can be seen, the reflectivity spectra fall into two groups, one corresponding to low $InO_{1.5}$ concentrations and the other to high concentrations. From 2 to about 13 m/o of $InO_{1.5}$, there is a single plasma band, modeled by a Drude term, having a maximum intensity at 2 m/o and decreasing in intensity as the electrical conductivity increases (Table A1). Between 400 and 600 cm^{-1} single polar phonon is seen. (The fitting procedure of the data is presented in the supplementary material.[25]) In contrast, from about 13 to 33 m/o of $InO_{1.5}$, the same composition over which the superlattices form, the plasmon band intensity increases continuously, exhibiting a maximum at a composition of 33 m/o $InO_{1.5}$. In addition, with increasing $InO_{1.5}$ concentration, three new phonons appear active in the IR spectra with frequencies near 220, 360, and 620 cm^{-1}.

Compared to the Raman spectra, where only zone center phonons can be observed, the IR spectra are dominated by the plasmon reflectivity, sometimes obscuring other features at low frequencies. Nevertheless, the IR spectra confirm the existence of new polar modes in the superlattices. These modes are limited in number and are apparently different from those expected from a distinct, second phase of In_2O_3 sesquioxide[26] (see Sec. IV). An alternative is that the interface modes give

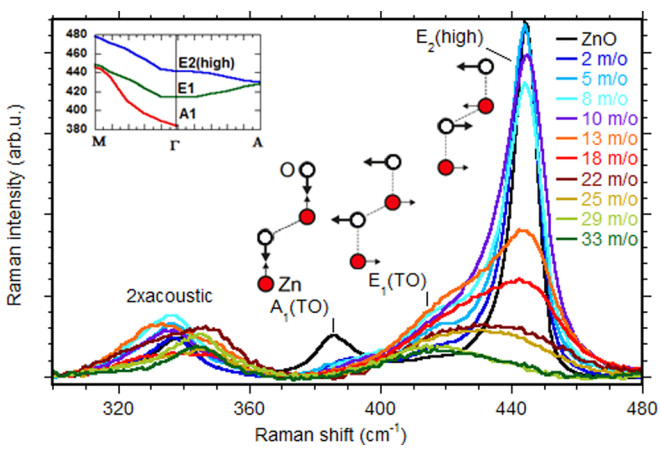

FIG. 5. Visible Raman spectra (excited at 532 nm) in the 390–410 cm^{-1} range showing A_1, E_1, and E_2 (high) ZnO phonons. The non-polar E_2 (high) mode shows characterisic features of phonon confinement with indium oxide concentration. Two regimes are observed: up to 10 m/o a volumetric confinement and above 13 m/o $InO_{1.5}$ a superlattice confinement indicated by the merging E_1 and E_2 (high) out of the Brillouin zone along k_z-axis.

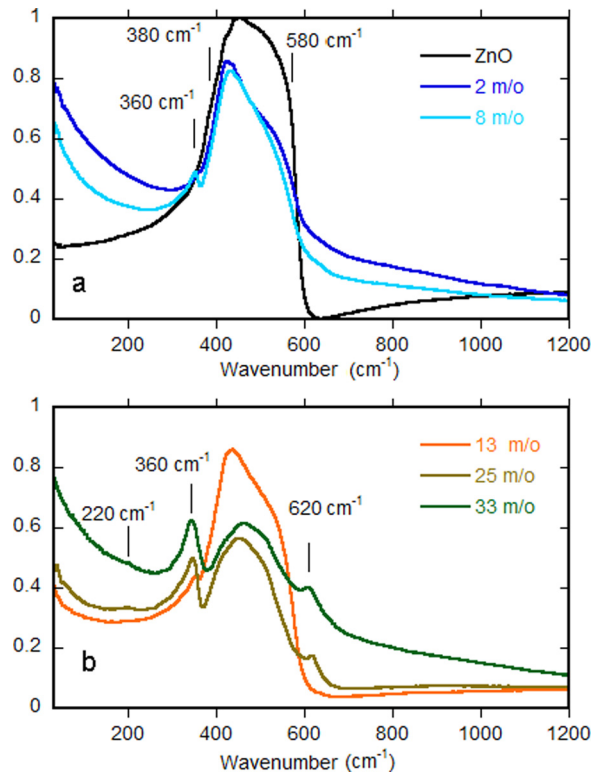

FIG. 6. Infrared reflectivity spectra for indium concentrations (a) below the formation of superlattices at about 13 m/o $InO_{1.5}$ (top) and (b) at higher concentrations at which superlattices form (bottom). Frequencies of IR active modes are listed in Table A1 and Raman mode frequencies are indicated in the figure.

rise to a strong dipolar contribution. As indicated by the values in Table A1, there is a correlation between the plasma band contribution and the electrical conductivity measurements. It has to be emphasized, though, that the reflectivity measurements are macroscopic and also made in unpolarized conditions. Consequently, they correspond to an averaging of anisotropic contributions from many differently oriented grains; this undoubtedly results in some uncertainties associated with the fitting.

The most striking observation of the low frequency Raman scattering measurements is the appearance of mode confinement by the superlattice. These are shown in Fig. 7, where the low frequency Raman spectra, excited with a 514.5 nm laser, have been obtained between 6 and 150 cm^{-1}. The E_2 (low) mode seen at 100 cm^{-1} in pure ZnO shows a decay and splitting into several branches corresponding to the dispersion of phonons in the Brillouin zone along the *c*-axis similar to the optical phonons in Fig. 5. Meanwhile, the low frequency spectra of the superlattices show also that above 13 m/o, new modes appear. None of these new modes corresponds to the phonons in single-crystal ZnO or In_2O_3, and therefore we explain them by the activation of acoustic phonons due to folding of the Brillouin zone.[27,28] Indeed, the modulation of the wave vector by the lattice folding of $(ZnO)_k/InO_2/(Zn0)_k$ results in a reduction of the Brillouin zone and the formation of a mini-Brillouin zone. For illustration, the effect of folding by $(k+1)$ equal to 7, 10, and 13 is shown in Fig. 7 based on the phonon spectrum for bulk ZnO.[22] They reasonably well reproduce the phonon modes observed experimentally. Some of the acoustic modes exhibit clear splitting, but the observation and identification of all the peaks is, however, not trivial, as the laser beam is focused into different randomly oriented grains in the samples. Furthermore, the X-ray diffraction data of Table I show that several samples contained a mixture of two different superlattices which would invariably produce spatial nonuniformities across the samples. Moreover, the intensities of the folded acoustic modes depend not only on the superlattice spacing but also on the symmetries of acoustic waves and the photo-elastic interactions in the elastic continuum model and resonance.[20,27–30] It follows that some modes may not be seen and the values calculated do not correspond to the inverse value of *k* for the Brillouin zone[2] in Table I. Moreover, some modes could be acoustic or shear modes of the InO_2 layer.[31] For instance, a peak at 60 cm^{-1} appears in all spectra. In addition, the inelastic background of the acoustic spectra (Fig. 7) increases in a similar manner to the optical phonon intensity (Fig. 4) and results in a quasi-phonon density of states due to some contribution of vibrations out of the zone center.

IV. DISCUSSION

The vibrational properties of $ZnO–In_2O_3$ in the compositional range 13 to 33 m/o $InO_{1.5}$ exhibit several characteristic features of superlattice nanostructures. In particular, the dependence on superlattice periodicity, Brillouin zone folding, and activation of acoustic phonons in the Raman spectra. This phenomenon is attributed to the periodic spacing of the

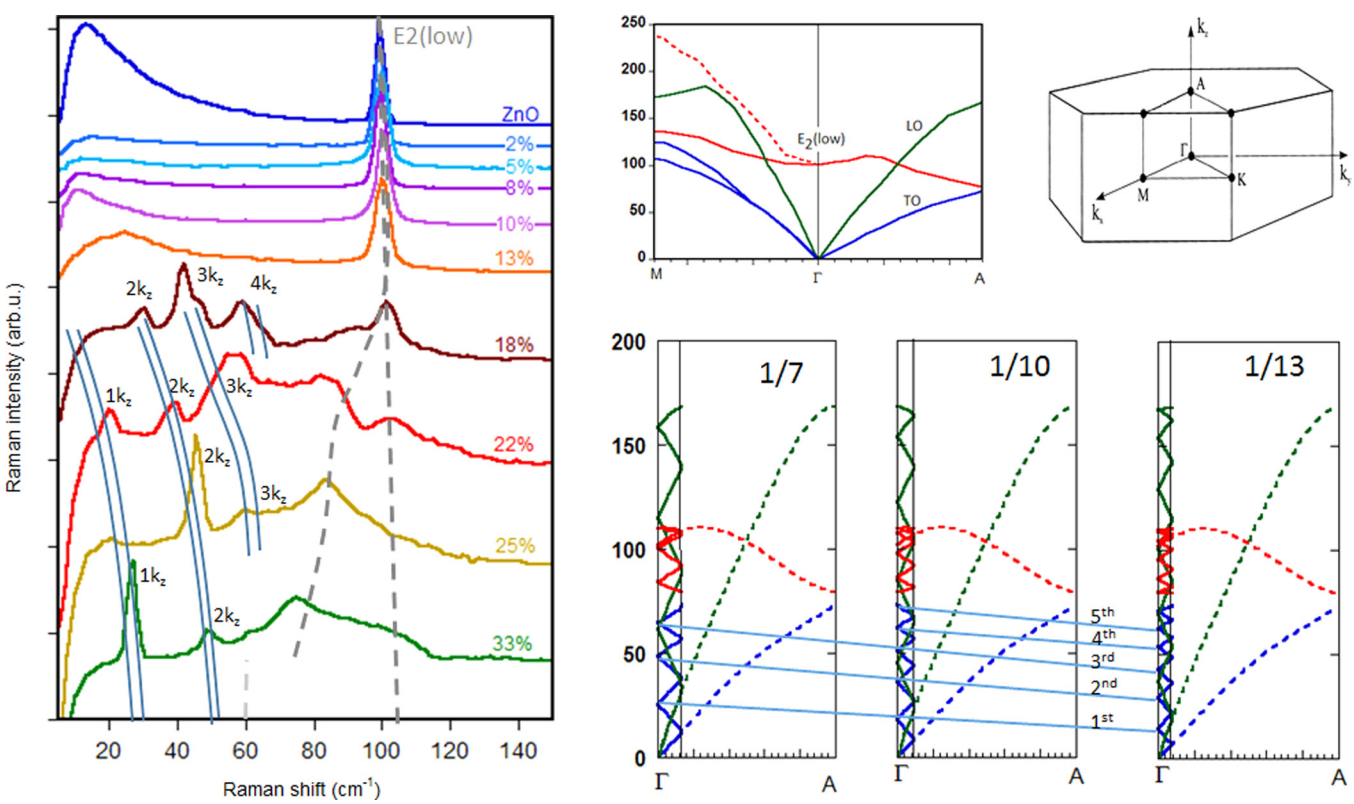

FIG. 7. Low frequency Raman spectra for different indium oxide concentrations. Rayleigh scattering is due to both free carrier scattering and additional modes due to the folding of acoustic branch in the Brillouin zone in the superlattice series. Top Right: reproduction of the dispersion of the vibrational modes redrawn from Serrano *et al.*[22] Lower right: calculated folding for different even (1/10) and odd values (1/7 and 1/13) based on the phonon spectrum.

InO_2 sheets separating $(ZnO)_k$ layers as observed by TEM and XRD. The vibrational spectra also express new modes at 520 and 620 cm^{-1} observed by Raman scattering (Fig. 4) and at 220, 350, and 600–628 cm^{-1} by IR reflectivity (Fig. 6). As these modes are not present in either pure ZnO or In_2O_3, our discussion is focused on two-dimensional vibrations of the $(ZnO)_kInO_2$ interface and plasmon coupling between electrons in the ZnO blocks and the InO_2 sheets.

A. InO_6 octahedral modes

To identify the possible vibrational modes, we first consider the vibrational modes of InO_6 octahedra in different oxide systems. Modelling of indium oxide clusters In_mO_n has shown that the most energetically favorable cluster corresponds to InO_6 octahedra whose mode frequencies are at 90, 117, 224, 228, 431, 478, 516, 543, and 596 cm^{-1}.[32] Isolated vibrations of InO_6 octahedra have also been measured in hydroxides with different octahedral environments.[33] The vibrational mode frequencies of InOOH, in which InO_6 octahedra are connected by corner-sharing, have been observed at 173, 540, and 612 cm^{-1}. As for $In(OH)_3$, where InO_6 octahedra are linked to one another by edge sharing, the vibrational mode frequencies are observed at 183 and 665 cm^{-1}.[33] The infrared mode at 360 cm^{-1} can be assigned to the bending mode of O–In–O octahedra.[26,34,35] In contrast, a mode at 620 cm^{-1} can be attributed to the stretching of In–O bonds.[35] For comparison, 22 Raman-active vibrational modes are predicted in sesquioxide crystals of In_2O_3.[26] Simulation and experimental data of internal modes give A_g at 576 cm^{-1} (not observed), E_g at 590 cm^{-1}, and T_g at 600 cm^{-1} (observed at 628 cm^{-1} (Ref. 26)). The vibrational energy of this mode is, however, quite sensitive to its surrounding and bonding. Indeed, Wang *et al.*[34] observed that the calculated frequency scales with the bulk modulus. Together, these findings suggest that the internal stretching of In–O mode is probably highly sensitive to the local indium–oxygen potential used in the calculation.[26,36] Meanwhile, the modes of InO_6 have to be compatible with the two-dimensional symmetry of the InO_2 sheets.

B. InO_2 two-dimensional layer modes

An isolated InO_2 sheet consists of InO_6 octahedra arranged in two-dimensional lattice with CdI_2 symmetry (Fig. 1). The corner-sharing octahedra present T_{2g} distortion along (111) axis and the sheet has D_3 symmetry.[37] The diperiodic group is DP72-D3/3d according to Woods[38] which leads to 6 zone center modes[39]

$$\Gamma = A_{1g} + E_g + 2A_{2u} + 2E_u$$

consisting of two acoustic modes, $A_{2u}(A) + E_u(A)$, two IR modes, $A_{2u}(IR) + E_u(IR)$, and two Raman modes $A_{1g}(R) + E_g(R)$. This two-dimensional model for the InO_2 sheets indicates that there can be only a limited number of allowed vibrational modes. However, there is an apparent inconsistency between the number of modes observed in Raman and IR spectra; IR gives three modes at 220, 350, and 600–628 cm^{-1} while Raman shows two modes at 520 and 620 cm^{-1}.

Interestingly, the 620 cm^{-1} mode exhibits a constant frequency and high intensity in the Raman scattering as a function of $InO_{1.5}$, while, in the IR spectra, it has a weaker intensity than the ZnO modes and its frequency depends on the indium content (Table S1 in the supplementary material[25]). Zallen *et al.*[40] have proposed that the splitting of the ionic and electronic polarization in layered structures can activate silent modes in IR or Raman spectra. However, the low frequency dispersion in the infrared spectra may correspond to the existence of plasmon bands. The modes at 520/620 cm^{-1} would then correspond to the Raman active modes coupled to plasmons, while the IR modes at 220 and 350 cm^{-1} would then correspond to the A_u and E_u modes of the two-dimensional structure of the InO_2 layer.

C. ZnO/InO_2 Interface modes

Evidence for the existence of ZnO/InO_2 interface modes comes from fitting of the IR reflectivity spectra. (The fitting procedure and simulations are described in the supplementary material.[25]) The simulation concerns a composite material consisting of a conductive material, corresponding to a single mode of ZnO, and a dielectric material with In–O vibration modes. The simulation included variations of the plasma band frequency and the In–O modes. These simulations predict that the sign inversion of the dielectric constant with $\varepsilon(ZnO) = -\varepsilon(InO_2)$ results at $Im(-1/\varepsilon(\omega)) = 0$ into the observation of an anomalous strong and broad peak around 500–700 cm^{-1}. More specifically, the addition of an In–O mode at 620 cm^{-1} results in a shift and peak splitting of the 580 cm^{-1} polar mode of ZnO into two peaks at 520 and 620 cm^{-1}, consistent with the observation. Although the modelling fit is excellent, it is based on assuming a plasma frequency of ~600 cm^{-1} in the Drude model which differs somewhat from the plasma frequency measured by infrared reflectivity (>2000 cm^{-1}, Table A1) and reported in doped ZnO (>6000 cm^{-1} (Ref. 41)). This latter plasma frequency is probably also related to the residual indium dopant in ZnO layers, present in all our samples, whereas the second plasma frequency of ~600 cm^{-1} matches exactly the phonon energy of InO_2. It is then supposely a coupled phonon-plasmon mode perpendicular to two-dimensional $(ZnO)_k/InO_2$ interface. The possibility of coupling of plasmons with longitudinal phonons in semiconducting and metal/dielectric superlattices dates back to the work of Mills.[42] The two branches, L− and L+, can be derived from the anisotropy of the dielectric function assuming that the plasmon frequency is localized by the InO_2 mode and they correspond to the 520 and 620 cm^{-1} frequencies (Fig. 4).

D. Possible origin of interface conductivity

The electrical conductivity of all the phases in the ZnO–In_2O_3 system is n-type due to the substitution of Zn^{2+} by In^{3+} ions. The room temperature electrical conductivities in Table I are in reasonable agreement with those reported for samples of similar composition grown by different techniques.[5,17,43–45] These are all degenerate semiconductors

having metallic-like conductivity with a doping of 10^{19}–$10^{21}\,cm^{-3}$. The formation (by precipitation) of random clusters or sheets of InO_2 is consistent with the decrease of electronic mobility[17,43,46] as well as the apparent saturation of the doping between about 10 and 18 m/o of $InO_{1.5}$. However, the increase of conductivity and mobility in the $ZnO_k(In_2O_3)$ single crystal (Table I, [3,17]) above about 13 m/o of InO_2 would be unexpected if only due to point defects. The increase in conductivity observed here coincides with the formation of the superlattices suggesting that the increase is associated with a high electron conductivity parallel to the superlattice planes. This is also consistent with the high-temperature conductivity of polycrystalline samples at 800 °C which increases with the number density of InO_2 sheets.[8] In the only single crystal study of transport anisotropy, Malochkin *et al.*[7] found that the electron conductivity of a single crystal flake of $(ZnO)_5In_2O_3$ is highly anisotropic, with the in-plane conductivity being two orders of magnitude higher along the *c*-axis. We conclude that the two-dimensional structure of InO_2 can be correlated to the in-plane conductivity.

V. CONCLUSIONS

ZnO–In_2O_3 ceramics, with compositions ranging from pure ZnO to 33 m/o $InO_{1.5}$, has been characterized by photoluminescence, optical and IR reflectivities, resonant and non-resonant Raman scattering, as well as low-frequency Raman scattering. Superlattice structures of $(ZnO)_kIn_2O_3$, well known to exist from TEM and XRD studies, give rise to Brillouin zone folding and activation of acoustic phonons, phonon confinement, selective resonances by Fröhlich interaction of $(ZnO)_k$ layers, as well as the band gap decrease by multi-quantum wells hybridization. In addition, new vibrational modes at 520 and 620 cm^{-1}, not present in either ZnO or bulk In_2O_3, are observed under non-resonant Raman scattering conditions. These are attributed to two-dimensional interface plasmon collective modes localized at the $(ZnO)_k/InO_2$ interface. The crystallography of the interface structure with the reversal of the polarity of the ZnO blocks on either side of the InO_2 layer also implies that there is a sign inversion in the dielectric constant. There is also the possibility, yet to be confirmed experimentally, of there being a two-dimensional electron gas at the superlattice interfaces due to a combination of spontaneous polarization induced charging at the interfaces and the band alignment of ZnO and InO_2 levels.

ACKNOWLEDGMENTS

The authors are grateful to Alban Maertens for assistance with the Hall and conductivity measurements. The work in Prague was supported by the Czech Science Foundation Project No. 15-08389S. S.S. was supported by EU funding under the 7th Framework Programme (Project NOTEDEV).

[1]H. Kasper, "News phases with the wurtzite structure in the ZnO-In_2O_3 system," Z. Anorg. Allg. Chem. **349**(3–4), 113–123 (1967).
[2]N. Kimizuka, M. Isobe, and M. Nakamura, "Syntheses and Single-crystal Data of Homologous Compounds $In_2O_3(ZnO)_m$ (m = 3,4,5), $InGaO_3(ZnO)_3$ and $Ga_2O_3(ZnO)_m$ (m = 7,8,9 and 16) in the In_2O_3–$ZnGa_2O_4$–ZnO System," J. Solid State Chem. **116**, 170–178 (1995).
[3]T. Moriga *et al.*, "Phase relationships and physical properties of homologous compounds in the zinc oxide–indium oxide system," J. Am. Ceram. Soc. **81**(5), 1310–1316 (1998).
[4]S. P. Harvey, K. R. Poeppelmeier, and T. O. Mason, "Subsolidus phase relationships in the ZnO–In_2O_3–SnO_2 system," J. Am. Ceram. Soc. **91**(11), 3683–3689 (2008).
[5]E. M. Hopper *et al.*, "Electronic and thermoelectric analysis of phases in the $In_2O_3(ZnO)_k$ system," J. Appl. Phys. **109**, 013713 (2011).
[6]Y. Masuda *et al.*, "Structure and thermoelectric transport properties of isoelectronically substituted $(ZnO)_5In_2O_3$," J. Solid State Chem. **150**, 221–227 (2000).
[7]O. Malochkin, W.-S. Seo, and K. Koumoto, "Thermoelectric properties of $(ZnO)_5In_2O_3$ single crystal grown by a flux method," Jpn. J. Appl. Phys., Part 2 **43**(2), L194–L196 (2004).
[8]X. Liang and D. R. Clarke, "Relation between thermolectric properties and phase equilibria in the ZnO–In_2O_3 binary system," Acta Mater. **63**, 191–201 (2014).
[9]M. Gaultois *et al.*, "A data-driven review of thermoelectric materials: Performance and resource considerations," Chem. Mater. **25**(15), 2911–2920 (2013).
[10]A. Nag and V. Shubha, "Oxide thermoelectric materials: A structure–property relationship," J. Electron. Mater. **43**(4), 962–977 (2014).
[11]M. Backhaus-Ricoult *et al.*, "Semiconducting large band gap oxides as potential thermoelectric materials for high-temperature power generation?," Appl. Phys. A **116**(2), 433–470 (2014).
[12]X. Liang, *Structure and Thermoelectric Properties of ZnO Based Materials* (Harvard University, USA, 2013).
[13]X. Liang, M. Baram, and D. R. Clarke, "Thermal (Kapitza) resistance of interfaces in compositional dependent ZnO–In_2O_3 superlattices," Appl. Phys. Lett. **102**, 223903 (2013).
[14]D. P. Li, G. Z. Wang, and X. H. Han, "Raman property of In doped ZnO superlattice nanoribbons," J. Phys. D: Appl. Phys. **42**, 175308 (2009).
[15]F. Urbach, "The long-wavelength edge of photographic sensitivity and of the electronic absorption of solids," Phys. Rev. **92**, 1324 (1953).
[16]K. Mahmood, S. B. Park, and H. J. Sung, "Enhanced photoluminescence, Raman spectra and field emission behavior of indium-doped ZnO nanostructures," J. Mater. Chem. C **1**, 3138–3149 (2013).
[17]N. Naghavi *et al.*, "Structural and physical characterisation of transparent conducting pulsed laser deposited In_2O_3-ZnO thin fillms," Mater. Chem. **10**, 2315–2319 (2000).
[18]P. Prathap *et al.*, "Growth and characterization of indium oxide films," Curr. Appl. Phys. **8**(2), 120–127 (2008).
[19]X. Zhang *et al.*, "Crystal structure of $In_2O_3(ZnO)_m$ superlattice wires and their photoluminescence properties," Cryst. Growth Des. **9**(1), 364–367 (2009).
[20]P. Y. A. M. Cardona, *Fundamentals of Semiconductors: Physics and Materials Properties Graduate Texts in Physics*, 4th ed. (Springer, 2010).
[21]T. C. Damen, S. P. S. Porto, and B. Tell, "Raman effect in zinc oxide," Phys. Rev. **142**(2), 570–574 (1966).
[22]J. Serrano *et al.*, "Dependence of phonon widths on pressure and isotopic mass: ZnO," Phys. Status Solidi B **235**, 260–266 (2003).
[23]R. Cuscó *et al.*, "Temperature dependence of Raman scattering in ZnO," Phys. Rev. B **75**, 165202 (2007).
[24]P. Parayanthal and F. H. Pollack, "Raman scattering in alloys semiconductors: Spatial correlation Model," Phys. Rev. Lett. **52**(20), 1822–1825 (1984).
[25]See supplementary material at http://dx.doi.org/10.1063/1.4950789 for IR data fitting.
[26]B. Garcia-Domene *et al.*, "High-pressure lattice dynamical study of bulk and nanocrystalline In_2O_3," J. Appl. Phys. **112**, 123511 (2012).
[27]M. Trigo, A. Feisntein, and B. Jusserand, "Finite-size effects on acoustic phonons in GaAs/AlAs superlattices," Phys. Rev. B **66**(12), 125311 (2002).
[28]A. Fainstein and B. Jusserand, "Raman scattering in resonant cavities," in *Light Scattering in Solid IX*, edited by R. M. M. Cardona (Springer-Verlag, Berlin, 2007).
[29]C. Colvard *et al.*, "Folded acoustic and quantized optic phonons in (GaAl)As superlattices," Phys. Rev. B **31**(4), 2080–2091 (1985).
[30]B. Jusserand "Selective resonant interaction between confined excitons and folded acoustic phonons in GaAs/AlAs multi-quantum wells," Appl. Phys. Lett. **103**, 093112 (2013).

[31]M. Boukhicha *et al.*, "Anharmonic phonons in few-layer MoS_2: Raman spectroscopy of ultralow energy compression and shear modes," Phys. Rev. B **87**, 195316 (2013).
[32]X. Mao-Jie *et al.*, "Structural, electronic and vibrational properties of indium oxide clusters," Chin. Phys. B **20**(6), 063101 (2011).
[33]X. Xue and M. Kanzaki, "High-pressure δ-$Al(OH)_3$ and δ-AlOOH phases and isostructural hydroxides/oxyhydroxides: New structural insights from high-resolution ^1H and ^{27}Al NMR," J. Phys. Chem. B **111**, 13156 (2007).
[34]C. Y. Wang *et al.*, "Phase stabilization and phonon properties of single crystalline, rhombohedral indium oxide," Cryst. Growth Des. **8**(4), 1257–1260 (2008).
[35]H. L. Zheng *et al.*, "Vibrational spectra of $CaGa_2O_4$, Ca_2GeO_4, $CaIn_2O_4$ and $CaSnO_3$ prepared by electrospinning," Appl. Phys. A **108**, 465–473 (2012).
[36]S. Mukhopadhyay *et al.*, "Theoretical study of small clusters of indium oxide: InO, In_2O, InO_2, In_2O_2," J. Mol. Struct. Theochem. **948**, 31–35 (2010).
[37]C. Schinzer, F. Heyd, and S. F. Matar, "$Zn_3In_2O_6$—Crystallographic and electronic structure," J. Mater. Chem. C **9**, 1569–1573 (1999).
[38]E. A. Wood, "The 80 diperiodic groups in three dimensions," Bell Syst. Tech. J. **43**, 541–559 (1964).
[39]A. Burneau, "Infrared and Raman selection rules in diperiodic three-dimensional layers," J. Raman Spectrosc. **25**, 289–301 (1994).
[40]R. Zallen, M. L. Slade, and A. T. Ward, "Lattice vibrations and interlayer interactions in crystalline As_2S_3 and As_2Se_3," Phys. Rev. B **3**(12), 4257–4273 (1971).
[41]T. Wang *et al.*, "Ultrabroadband terahertz conductivity of highly doped ZnO and ITO," Opt. Mater. Express **5**(3), 566–575 (2015).
[42]D. L. Mills, "Collective excitations in superlattice structures," in *Light Scattering in Solids V* (Springer–Verlag, 1989).
[43]S.-Y. Lee and B.-O. Park, "Electrical and optical properties of In_2O_3–ZnO thin films prepared by sol–gel method," Thin Solid Films **484**(1–2), 184–187 (2005).
[44]H. Peng *et al.*, "Possible n-type carrier sources in $In_2O_3(ZnO)_k$," Chem. Mater. **24**(1), 106–114 (2012).
[45]A. C. Galca, G. Socol, and V. Craciun, "Optical properties of amorphous-like indium zinc oxide and indium gallium zinc oxide thin films," Thin Solid Films **520**(14), 4722–4725 (2012).
[46]K. Ellmer and R. Mientus, "Carrier transport in polycrystalline transparent conductive oxides: A comparative study of zinc oxide and indium oxide," Thin Solid Films **516**(14), 4620–4627 (2008).